Simulation of Power Exhaust in Edge and Divertor of the SlimCS Tokamak Demo Reactor

Nobuyuki ASAKURA, Katsuhiro SHIMIZU, Hisato KAWASHIMA, Kenji TOBITA
and Tomonori TAKIZUKA

Japan Atomic Energy Agency, Naka, Ibaraki 311-0193 Japan

Design of the power handling for the demo tokamak reactor, SlimCS, with the fusion power of $P_{fus} \leq 3$ GW and the exhausted power of $P_{out} = 500$ MW was investigated. First, effects of the divertor geometry of the V-shaped corner and the Ar impurity seeding on the radiation distribution and the target power loading were summarized in the simulation (SOLDOR/NEUT2D) with a constant concentration of Ar ions. Second, influence of the intense Ar impurity seeding was investigated in SONIC code, using Monte Carlo calculation (IMPMC). In this work, Ar transport and plasma evolution were self-consistently simulated up to a typical transport time in the divertor ($t = 30$ ms). Results showed that Ar density and its concentration were significantly increased and their peaks were rather localized near the target. Influence of both n_e and n_{Ar} enhancement on the peak power loading was significant in the full detached divertor, where $q_{target} = 18$ MW/m^2 was attributed to the radiation power and was two times larger than the previous work. Further calculation up to a quasi-steady-state is necessary to obtain impurity and radiation distributions at the upstream of the divertor, SOL and edge.

Keywords: SlimCS, Tokamak, Demo reactor, Divertor, SONIC, Power handling, Impurity seeding, Detachment

1. Introduction

Handling of a large exhausted power is the most important issue for the fusion reactor design, which requires an integration of the edge and divertor plasma physics, plasma material interaction, and technology of the high temperature components. For the demo rector, the exhausted power from the core plasma (P_{out}) becomes large such as several 100 MW compared to those in existing large tokamaks (several MW to a few 10 MW) and ITER (about 100 MW) [1]. For the development of the plasma operation scenario and divertor design, the total radiation loss fraction (P_{rad}^{tot}/P_{out}) of more than 90 % is required in the edge and divertor.

Divertor design for the power handling in the tokamak demo reactor, SlimCS [2, 3], has recently progressed, using two-dimensional plasma fluid code (SOLDOR) and neutral Monte Carlo code (NEUT2D) [4], where the non-coronal radiation model (radiation power function) [5] was used and the impurity concentration of Ar (n_{Ar}/n_i) was increased. Impurity Monte Carlo code (IMPMC) has advantages for impurity modelling since most kinetic effects on the impurity ions such as thermal and friction forces along the magnetic field are incorporated in original formula. It was recently incorporated with SOLDOR and NEUT2D codes, and

self-consistent coupling between the three codes was established in the integrated divertor code, SONIC, for low Z ions such as helium and carbon [6-8].

In this paper, summary of the SOLDOR/NEUT2D simulation in the SlimCS divertor and the application of the SONIC code with the intensive Ar seeding are presented. A design work of the SlimCS divertor and simulation results are summarized in Section 2. Development of the SONIC for the Ar impurity transport and the first result are shown in Section 3. Summary and issues for the power handling scenario for the Demo reactor are presented in Section 4.

2. Power Exhaust Simulation in a SlimCS Divertor

2.1 Divertor design for power exhaust simulation

SlimCS is a conceptual DEMO design of a low aspect ratio tokamak ($R/a = 2.6$ with a reduced-size Central Solenoid coils) for the steady-state operation with the core dimension similar to those in ITER, power generation capability of a giga-watt level, and, at the same time, taking into account economical prospect towards commercialization. Figure 1(a) shows poloidal cross-section of the plasma. Plasma parameters in the recent design [3] are the major radius $R_p = 5.5$ m, the

minor radius $a_p = 2.1$ m, the plasma current $I_p = 16.7$ MA, toroidal field $B_t = 6.0$ T, ellipticity $\kappa_{95} = 2.0$, triangularity $\delta_{95} = 0.35$, and plasma volume $V_p = 941$ m^3. For the fusion power of $P_{fus} \leq 3$ GW, the total heating power of $P_{heat} \sim 600$ MW and $P_{out} \sim 500$MW are expected.
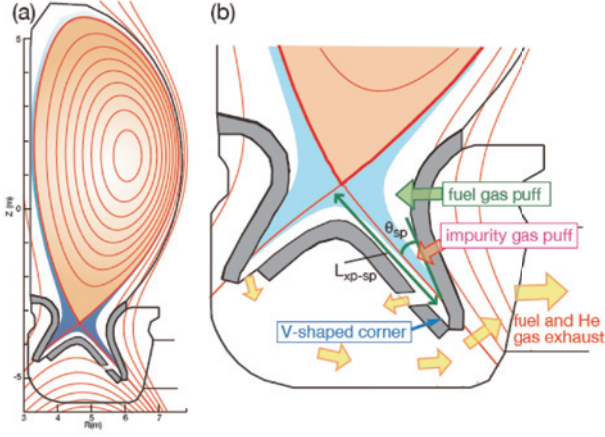

Fig.1 (a) Cross-section of the SlimCS plasma configuration and divertor. (b) Enlarged illustration of plasma configuration and the divertor geometry.

Figure 1(b) shows cross-section of the SlimCS divertor, which was proposed in Reference 4. The basic design concept for the ITER divertor, i.e. formation and control of detachment of the divertor plasma, is applied. At the same time, in order to reduce the peak heat load, effects of the divertor geometry on the power and particle handling are enhanced: (1) divertor leg is longer (inner $L_{xp-sp} = 1.37$ m, outer $L_{xp-sp} = 1.83$ m) and inclination of the target (inner $\theta_{sp} = 21°$, outer $\theta_{sp} = 18°$) is larger than those in ITER (inner $L_{xp-sp} = 0.97$ m and $\theta_{sp} = 38°$, outer $L_{xp-sp} = 1.14$ m and $\theta_{sp} = 25°$) to increase particle recycling and radiation power efficiently along the divertor leg, (2) a private dome is installed to increase the neutral pressure for exhaust of tritium gas and helium ash from the private flux region, (3) the outer exhaust slot is allocated between 20 and 40 cm above the bottom of the divertor, which will efficiently produce plasma detachment near the strike-point in the V-shaped corner.

At the same time, intense impurity seeding is required to increase the radiation loss over a wide range of the plasma edge, SOL and divertor. For the first study of the divertor simulation by the SOLDOR/NEUT2D codes, Ar seeding was used assuming the impurity concentration. Radiation loss in the outer divertor was increased with increasing a ratio of n_{Ar}/n_i from 2 to 5 %, while a constant value of $n_{Ar}/n_i = 1$% was assumed in the inner divertor and edge regions. Here, the radiation power function of Ar ions is less sensitive to the electron temperature range between a few 10 and a few 100 eV, compared to that of lower Z gasses such as Ne and N$_2$, which have a peak at 20 – 50 eV [5]. Thus, the Ar seeding is expected to increase the radiation loss both in the main

and divertor plasmas and thereby have an advantage to control the radiation loss under the condition of variable temperature in the SOL and divertor.

2.2 Divertor geometry effects

Effect of the target geometry, i.e. "V-corner", on the radiation power and the power loading profile was investigated in the different geometries as shown in Fig. 2. For Case-1 and Case-2, the outer exhaust slot is located at the bottom of the divertor and at 20 cm above the bottom, respectively. Here, core plasma boundary ("edge") for the calculation is set at $r/a = 0.95$, where $P_{out} = 500$ MW and total ion flux of $\Gamma_{out} = 5 \times 10^{22}$ D/s are exhausted. Gas puff of $\Gamma_{puff} = 1 \times 10^{23}$ D/s (~ 200 Pa·m3/s) is injected at the outer divertor throat as shown in Figure 1(b). Thermal diffusivities of electron and ion, $\chi_{e\perp} = \chi_{i\perp} = 1$ m^2/s, and particle diffusion coefficient, $D_\perp = 0.3$ m^2/s, are constant in the edge and SOL similar to those in the ITER simulation [9]. The pumping speed ($S_{pump} = 200$ m^3/s) is specified at the exhaust port of the divertor, i.e. right end of the calculation mesh.

When the location of the outer exhaust slot changed, the total particle recycling in the outer divertor is increased from 3.7×10^{24} D/s (Case-1) to 4.2×10^{24} D/s
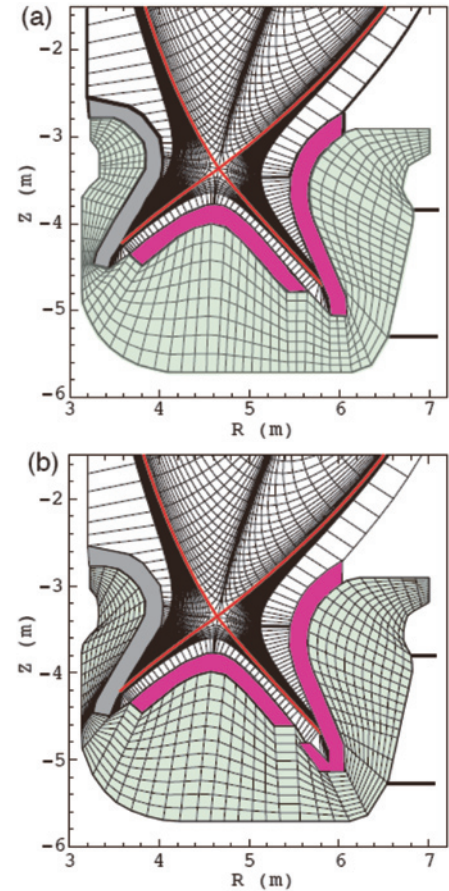

Fig.2 SOLDOR/NEUT2D calculation mesh for two divertor geometries: (a) Case-1 for the outer exhaust slot at the divertor bottom and (b) Case-2 for 20 cm above the bottom ("V-shaped corner").

(Case-2). Total radiation loss in the outer divertor (P_{rad}^{o-div}) is increased from 85 to 142 MW, which is caused by an significant increase in neutral recycling at upstream of the strike point. Contour plot of the radiation power at the upstream of the target for the Case-2 is presented in Figure 4(a). The total divertor radiation loss of $P_{rad}^{div} \sim 260$ MW is two times larger than the total edge radiation loss of $P_{rad}^{edge} \sim 130$ MW, and the total radiation loss (P_{rad}^{tot}) became 400 MW, corresponding to $P_{rad}^{tot}/P_{out} = 0.80$.

Heat load at the divertor target, q_{target}, is evaluated, including heat load due to radiation power flux (F_r) and neutral energy flux (F_n), by,

$$q_{target} = \gamma \cdot n_d C_{Sd} T_d + n_d C_{Sd} E_{ion} + F_r(P_{rad}) + F_n(\tfrac{1}{2} m_0 v_0^2 \cdot n_0 v_0), \quad (1)$$

where γ, n_d, C_{sd}, T_d, E_{ion} are sheath transmission coefficient, density, plasma sonic speed, temperature at the divertor sheath, surface recombination energy, respectively. The first term in the RHS corresponds to the total heat load transported by convection and conduction of electrons and ions. The second, third and forth terms are the surface recombination energy, radiation power from the divertor plasma, and neutral flux due to charge exchange and volume recombination, respectively.

to $T_e \sim 20$ eV and $T_i \sim 90$ eV for Case-2. As a result, due to the improvement of the divertor geometry to the "V-shaped corner", the recycling and radiation loss at the upstream are increased, and severe peak heat load of q_{target} ~ 70 MW/m^2 is decreased to 27 MW/m^2. This is caused by a reduction in the first term (plasma transport term) from 58 to 16 MW/m^2, while the total heat load by the radiation and neutral fluxes are comparable (14 MW/m^2).

2.3 Increase of Ar seeding

Next, Ar concentration at the outer divertor was increased in order to reduce the peak heat load lower than that for the ITER (10 MW/m^2), for the same divertor geometry of Case-2. It is found that the partially detached plasma extends to the outer flux surfaces for the case with $n_{Ar}/n_i = 5$ % (Case-3). Figure 4(b) shows that plasma area emitting intense radiation power extends to the outer and upstream in the divertor, compared to that in Figure 4(a). Plasma detachment also extends to the outer and upstream of the target. Here, P_{rad}^{o-div} and P_{rad}^{div} are significantly increased to 210 MW and 330 MW, respectively. P_{rad}^{tot} become 460 MW, corresponding to $P_{rad}^{tot}/P_{out} = 0.92$.

Profiles of the heat load at the outer target are presented in Figure 5 for the two cases. Components

Fig.4 Distribution of radiation power density in the outer divertor with Ar concentration of (a) $n_{Ar}/n_i = 2\%$ for Case-2, (b) $n_{Ar}/n_i = 5\%$ for Case-3. Ref.[4]
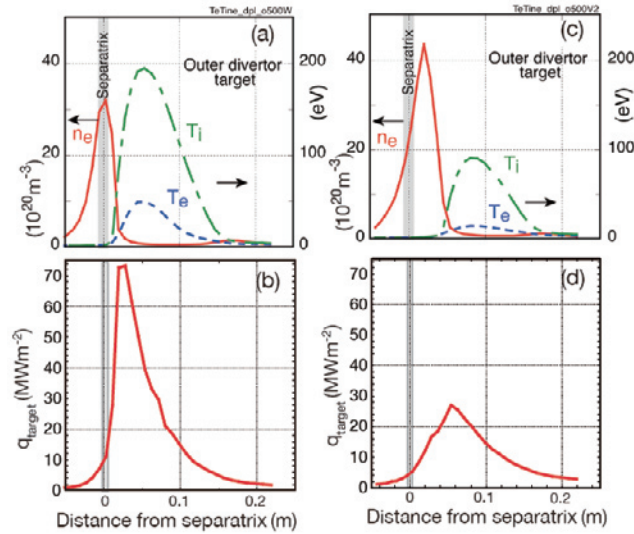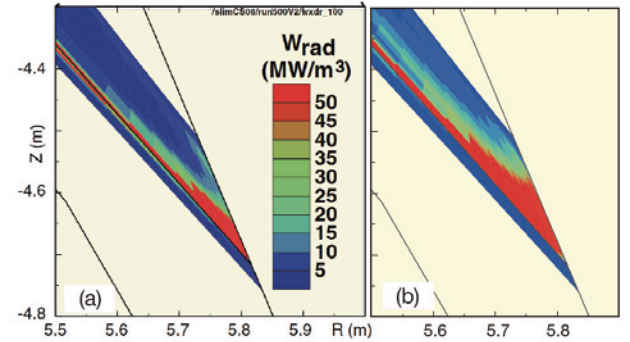

Fig.3 Calculation results in two divertor geometries: (a) profiles of plasma temperatures and electron density at the outer target for Case-1, and (b) heat load profile. (c) Profiles of plasma temperatures and electron density at the outer target for Case-2, and (d) heat load profile. Ref.[4]

Figure 3 shows that T_e and T_i near the strike point (< 2cm) are a few eV, where the plasma detachment is observed. On the other hand, peak $T_e \sim 50$ eV and $T_i \sim 200$ eV (for Case-1) are seen at the outer flux surfaces (~8cm from the strike-point), which is called as "partially detached divertor". These peak values are largely reduced
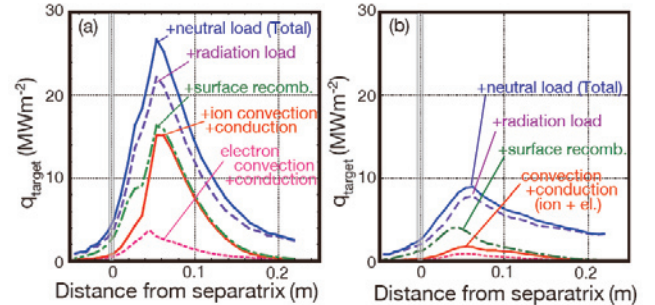

Fig.5 Profiles of the total heat load at the outer target and the components, (a) for Case-2 ($n_{Ar}/n_i = 2\%$), (b) for Case-3 ($n_{Ar}/n_i = 5\%$): electron and ion transport (convection and conduction) fluxes, surface recombination energy flux, radiation power load, and neutral load are shown.

corresponding heat loadings in Equation (1) are also shown. For the Case-3, i.e. with the V-shaped corner and intense Ar seeding, the transport heat load is significantly decreased to less than 2 MW/m^2 over the target plate, which is called as "full detached divertor". Peak heat load in the detached divertor is reduced to q_{target} ~9 MW/m^2, which is attributed mostly to the impurity radiation loss and surface recombination. Since the volume of the intense radiation loss is extending to the upstream, the radiation heat load is comparable for the two cases. Figure 6 summarizes two components of peak q_{target}, i.e. due to the plasma transport and due to radiation, neutral flux and surface recombination, as a function of $P_{rad}^{o\text{-}div}$.

For the power handling in the DEMO divertor, the total radiation fraction (P_{rad}^{tot}/P_{out}) of more than 90 % is required. At the same time, distribution of the radiation loss over the wide area in the edge and divertor should be established in order to avoid local overheating of the plasma facing components (PFCs) by the radiation loss.
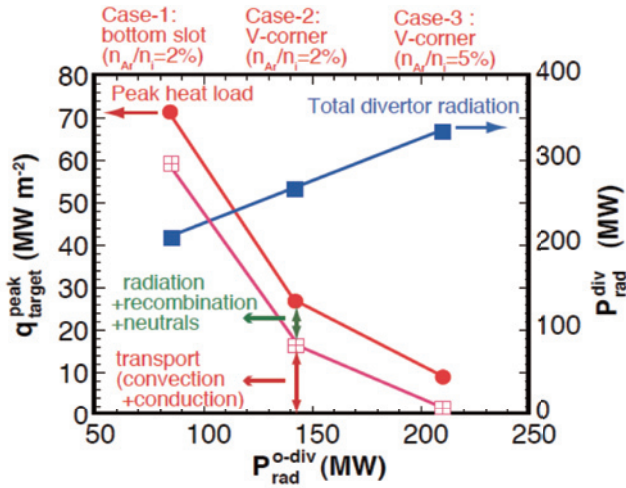

Fig.6 Peak heat lading at the outer target, q_{target}^{peak}, and total radiation power in the divertor, P_{rad}^{div}, as a function of total radiation power in the outer divertor, $P_{rad}^{o\text{-}div}$, for Case-1, Case-2 and Case-3.

3. Development of SONIC Simulation with Ar Seeding

Modelling and understanding of the seeding impurity transport in the edge and divertor are crucial for development of the power handling scenario. Recently, two-dimensional impurity Monte Carlo code (IMPMC) was incorporated with SOLDOR and NEUT2D, and impurity transport of low Z ions such as helium and carbon was investigated in SONIC code [8, 10]. Transport of Ar ions and atom in the DEMO divertor is, for the first time, investigated. At this stage, Ar impurity transport was simulated up to a typical time scale of the impurity transport in the divertor such as t = 30 ms, for the case of P_{out} = 500 MW, Γ_{out} = 5x10^{22} D/s, and fuel gas and Ar seeding fluxes of Γ_{puff} = 1x10^{23} D/s and Γ_{Ar} =

2x10^{21} Ar/s, respectively. Investigation of the high charged Ar transport to the upstream of the divertor, SOL and edge requires the further calculation time. Here, the time scale can be extended with increasing calculation time of the computer cluster, and about 9 hours was chosen for this study. Plasma equilibrium and the divertor geometry are the same as Case-2 and Case-3 ("V-shaped corner"). Self-consistent solutions of the SONIC simulations are obtained from two different initial plasma conditions: (Case-4) starting from partially detached divertor solution of Case-2, and (Case-5) starting from a full detached divertor solution with lower P_{out}.

3.1 Ar transport in the outer divertor

Transport of Ar atoms and ions was traced during the intense Ar seeding for Case-4. Figure 7 shows the SONIC simulation results at t = 30 ms, i.e. contour plots of electron temperature, ion and Ar ion densities, and Ar concentration in the outer divertor. Partially detached divertor is sustained as shown in Figure 8: T_e and T_i near the strike point (< 5 cm) are a few eV, while peak T_e ~30 eV and T_i ~110 eV are seen at the outer flux surfaces (~8 cm from the strike-point) and peak heat load q_{target} = 29
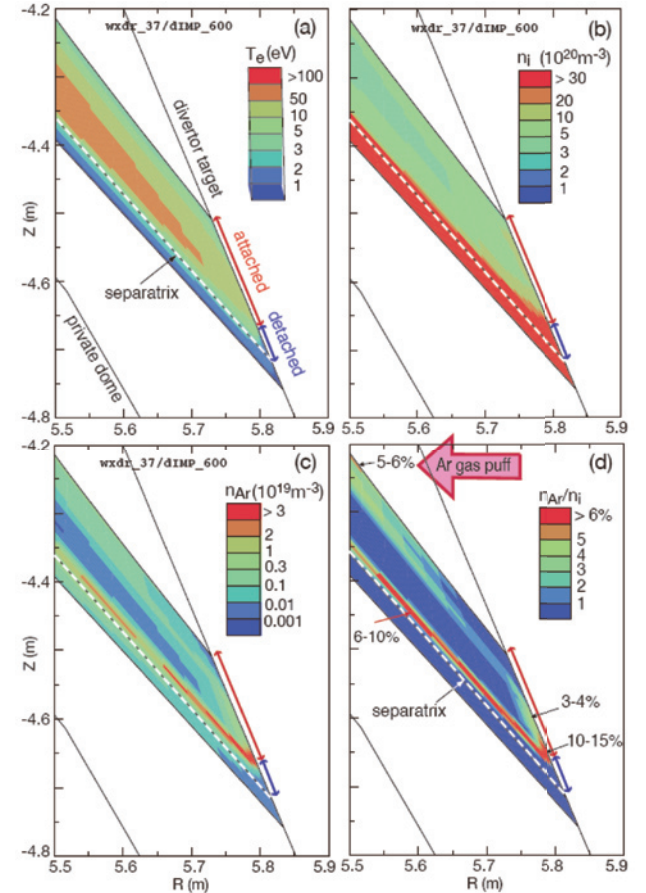

Fig.7 SONIC simulation result at t = 30 ms after starting a intense Ar seeding at upstream of the target (Case-4): distributions of (a) electron temperature in the outer divertor, (b) ion density, (c) Ar ion density, and (d) Ar concentration. Partially plasma detachment is seen at the target: up to 6 cm from the strike-point.
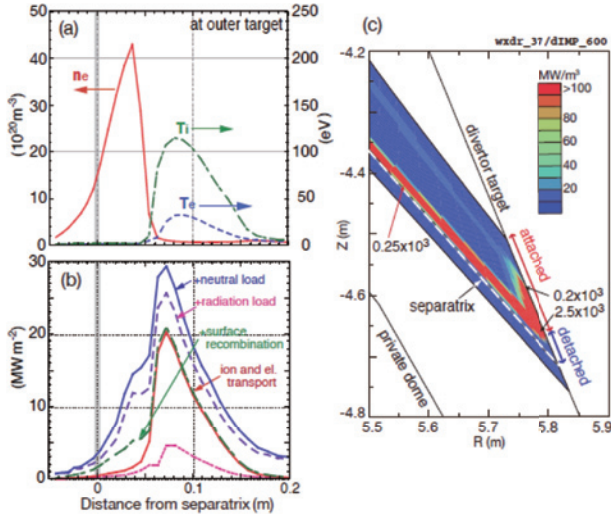
Fig.8 SONIC simulation for Case-4: profiles of (a) plasma temperatures and electron density at the outer target, and (b) heat load. (c) Distribution of radiation loss in the outer divertor. Each color corresponds to a value two times larger than that in Fig. 4, and radiation power densities are also shown.

MW/m^2, which are slightly larger than those in Case-2 (q_{target} = 27 MW/m^2).

Distribution of Ar ion concentration is presented in Figure 7(d). Ar ions are produced near the location of Ar gas puff, where n_{Ar}/n_i = 5-6 %, and they are transported towards the target along the field line due to a dominant friction force by the plasma flow. Ar recycling is enhanced near the target: n_{Ar}/n_i = 3-4 % at the downstream, and the maximum n_{Ar}/n_i = 10-15 % is seen near the boundary of the attached and detached plasmas. At the same time, large temperature gradient along the field line is produced at the upstream of the boundary such as T_e = 1-2 eV near the target and ~200 eV near the null point, thus Ar ions are carried towards the upstream by the intense thermal force: n_{Ar}/n_i = 6-10 % along the field lines. Figure 8(c) shows that radiation power density is enhanced above the target, and the peak values are about 10-15 times larger than those in Case-2 (non-coronal model with a constant n_{Ar}/n_i = 2 %). As a result, both the radiation power and n_{Ar}/n_i in the SONIC result are localized above the target. This is caused by a dominant friction force at the outer flux surfaces. Influence of the kinetic effect on Ar ions is observed in a narrow flux surfaces at the upstream of the attached and detached plasma boundary, where Ar recycling is significantly enhanced.

Next, transport of Ar was investigated for Case-5. Figure 9 shows contour plots of electron temperature, ion and Ar ion densities, and Ar concentration in the outer divertor at t = 30 ms. Full detached divertor is sustained as shown in Figure 10: both T_e and T_i at the outer flux surfaces are reduced to 2-3 eV, and peak heat load also

decreased to 18 MW/m^2. Ar density and its concentration are increased by the factors of 2–7 and 1.5–3, respectively,
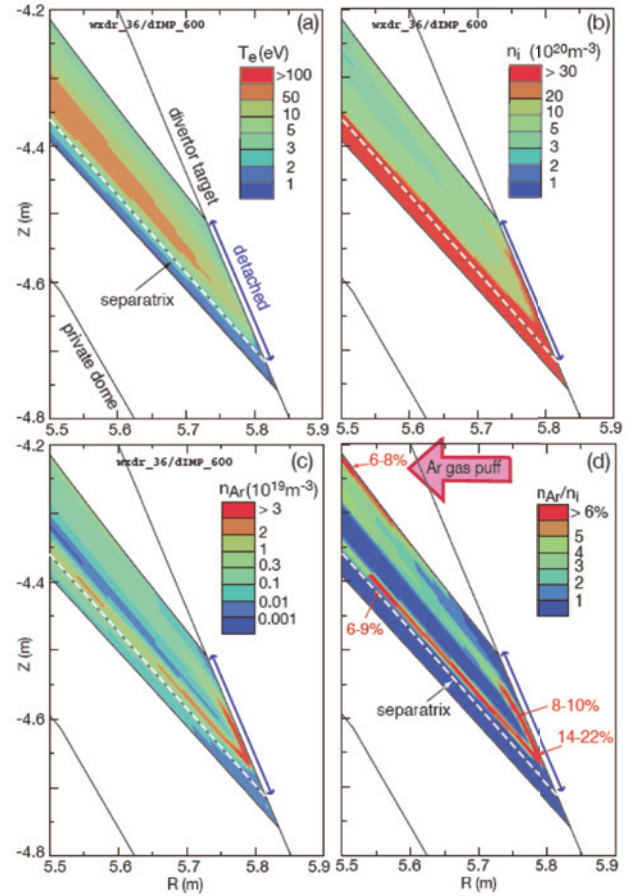

Fig.9 SONIC simulation result at t = 30 ms after starting a intense Ar seeding at upstream of the target, (Case-5): distributions of (a) electron temperature in the outer divertor, (b) ion density, (c) Ar ion density, (d) Ar concentration. Detachment is seen over the target.
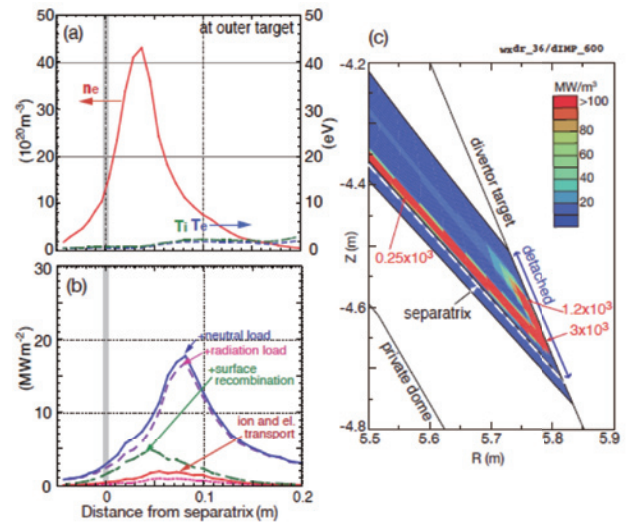

Fig.10 SONIC simulation for Case-5: profiles of (a) plasma temperatures and electron density at the outer target, and (b) heat load. (c) Distribution of radiation loss in the outer divertor. Each color corresponds to a value two times larger than that in Fig. 4.

over the wide area above the target, compared to Case-4. Figure 10(c) shows that radiation power density is also increased, in particular, at the outer flux surfaces (5 – 15 cm away from the strike-point) due to increase in both n_e and n_{Ar}. Here, the peak heat load in the full detached divertor is two times larger than that for Case-3 ($q_{target} \sim 9$ MW/m^2) mostly due to increase in the radiation heat load.

3.2 Power handling in SONIC results

Total radiation loss in the outer divertor and the peak heat load of the SONIC results are summarized in Figure 11. For the partially detached diveror of Case-4, P_{rad}^{o-div} = 177 MW is large compared to P_{rad}^{o-div} = 142 MW for the initial plasma condition (Case-2). On the other hand, the transport component of q_{target} is comparable for the two cases (15-16 MW/m^2). Although Ar impurity concentration and enhancement of the radiation power are localized for Case-4, the total radiation loss integrated along the flux surface upstream of q_{target} is comparable. Influence of the localization on the peak heat load is rather small.
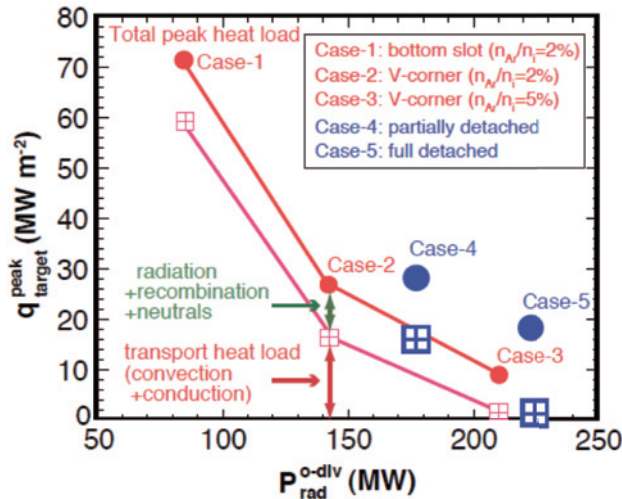

Fig.11 Peak heat loading at the outer target, q_{target}^{peak}, as a function of total radiation power in the outer divertor, P_{rad}^{o-div}, for the SONIC results (Case-4 and Case-5) are shown by large circles and squares, in addition to Case-1, Case-2 and Case-3.

For the full detached divertor of Case-5, P_{rad}^{o-div} = 223 MW is slightly large compared to P_{rad}^{o-div} = 210 MW in Case-3. The peak heat load of q_{target} = 18 MW/m^2 is two times larger than q_{target} = 9 MW/m^2 for Case-3, which is attributed mostly to the radiation heat load. Influence of the localization of both n_e and n_{Ar} on the peak heat load is significant in the full detached divertor plasma.

These two results are obtained in the same external parameters while the different initial conditions, which suggests that the self-consistent solutions of the plasma, neutrals and impurity are still transient in the upstream of the divertor, SOL and edge. Further simulation up to the particle confinement time such as a second will provide impurity and radiation distributions near a steady-state by

Ar ions with higher charge-states.

4. Summary and Future Development

A divertor simulation code (SONIC) has been developed for the divertor design of huge power handling (P_{out} = 500 MW) in the SlimCS DEMO reactor ($P_{fus} \leq 3$ GW). Previous work [4] proposed a divertor with a long-leg and V-shaped corner with an intense Ar impurity seeding. The SOLDOR/NEUT2D code simulation with $n_{Ar}/n_i \sim 5\%$ at the divertor could produce a detached divertor, where $P_{rad}^{div}/P_{out} \sim 66\%$ and $P_{rad}^{tot}/P_{out} \sim 92\%$. The peak heat load was reduced to $q_{target} \sim 9$MW/m^2, which was attributed mostly to power loadings by radiation and neutral flux, compared to the convection and conduction heat fluxes.

In this study, transport of Ar impurity was investigated in SONIC code, using Monte Carlo simulation (IMPMC). At this stage, Ar transport and plasma evolution were self-consistently simulated up to a typical transport time scale in the divertor such as t = 30 ms, for two different initial conditions, i.e. partially and fully detached divertor plasmas. In both cases, Ar density and its concentration were significantly increased and their peaks were localized near the target, compared to those in the previous results. Influence of enhancement of both n_e and n_{Ar} on the peak heat load was significant in the full detached divertor. q_{target} = 18 MW/m^2 is attributed to the radiation power loading, which was two times larger than the previous result. Influence of the friction force on the impurity against the thermal force, and their modeling by Monte Carlo calculation will be furthermore investigated.

Distribution of the radiation loss over a wide area, i.e. edge and divertor, is required in order to avoid local overheating of the plasma facing components. These self-consistent solutions of the plasma, neutrals and impurity are still transient in the upstream divertor, SOL and edge. Further extension of simulation up to the particle confinement time such as a second will be required to obtain impurity and radiation distributions in a quasi-steady-state by Ar ions with higher charge-states.

In the future DEMO divertor design, SONIC simulation will be developed to improve the design for the particle control in order to satisfy helium exhaust, as well as maintaining the divertor detachment in the high neutral pressure and radiation loss.

[1] M. Shimada, et al., Nucl. Fusion **47** (2007) S1.

[2] K. Tobita, et al., Nucl. Fusion **47** (2007) 892.

[3] K. Tobita, et al., Nucl. Fusion **49** (2009) 075029.

[4] H. Kawashima, et al., Nucl. Fusion **49** (2009) 065007.

[5] D. Post, et al., Phys. Plasmas **2** (1995) 2328.

[6] K. Shimizu, et al., J. Nucl. Mater. **313-316** (2003) 1277.

[7] H. Kawashima, et al., Plasma and Fusion Research: Regular Articles Volume 1, (2006) 031.

[8] K. Shimizu, et al., J. Nucl. Mater. **390-391** (2009) 307.

[9] A. S. Kukushkin, et al., J. Nucl. Mater. **337-339** (2005) 50.

[10] K. Shimizu, et al., Nucl. Fusion **49** (2009) 065028.